High-Throughput Synthesis of Graphene by Intercalation–Exfoliation of Graphite Oxide and Study of Ionic Screening in Graphene Transistor

Priscilla Kailian Ang,[†,§] Shuai Wang,[†] Qiaoliang Bao,[†] John T. L. Thong,[‡] and Kian Ping Loh[†,*]

[†]Department of Chemistry, National University of Singapore, 3 Science Drive 3, Singapore 117543, [‡]Department of Electrical and Computer Engineering, National University of Singapore, 4 Engineering Drive 3, Singapore 117576, and [§]NUS Graduate School for Integrative Sciences and Engineering, Singapore 117597

ABSTRACT We report a high-throughput method of generating graphene monolayer (>90% yield) from weakly oxidized, poorly dispersed graphite oxide (GO) aggregates. These large-sized GO aggregates consist of multilayer graphite flakes which are oxidized on the outer layers, while the inner layers consist of pristine or mildly oxidized graphene sheets. Intercalation–exfoliation of these GO aggregates by tetrabutylammonium cations yields large-sized conductive graphene sheets (mean sheet area of 330 ± 10 μm^2) with high monolayer yield. Thin-film field-effect transistors made from these graphene sheets exhibit high mobility upon nullifying Coulomb scattering by ionic screening. Ionic screening *versus* chemical doping effects of different ions such as chloride and fluoride on these graphene films were investigated with a combination of *in situ* Raman spectroscopy and transport measurement.

KEYWORDS: graphene · intercalation · exfoliation · ionic screening

Graphene-based nanoelectronic devices are of great interest because the active channel can be scaled literally down to a single crystalline sheet of sp^2-bonded carbon. Such devices can exhibit ultrahigh carrier mobility and long-range ballistic transport.[1,2] Currently, the "Scotch tape" peeling method used for producing graphene layers from graphite is not compatible with industrial production. The search is on for a high-yield production route toward high-purity, large-sized graphene sheets which can be deposited as a uniform film on substrate. Reported production methods are quite varied and range from the chemical and thermal reduction of graphite oxide,[3–5] liquid-phase intercalation and exfoliation of graphite,[6–10] and epitaxial growth[11,12] to chemical vapor deposition.[13] Of these, solution-processed graphene sheets offer low-cost and high-throughput for printable device fabrication on flexible substrates. The most commonly used Hummer's method produces aqueous solution of graphene oxide sheets, which are used as precursors to generate mildly conducting graphene films. However, the harsh oxidation method results in small-sized insulating graphene oxide sheets with widths in the submicrometer range.[3] For ease of device fabrication, it is desirable to synthesize graphene sheets with a lateral size larger than 20 μm.[5,14] Several researchers have demonstrated exfoliation and intercalation of graphite to produce monolayer graphene sheets.[6–10] However, these methods suffer from low yield (~1%) of monolayer sheets and sometimes involve the use of hazardous exfoliating or reducing agents such as oleum[6] and hydrazine.[4,5] Hence, a solution-phase method which can achieve high monolayer yield of large-sized conductive graphene sheets under mild conditions is highly desirable.

In this report, we present an efficient and highly reproducible one-step intercalation and exfoliation method to produce large-sized, conductive graphene sheets without the use of surfactants. By removing the ultrasonication step completely, we are able to obtain large-sized exfoliated graphene sheets (with lateral dimension >20 μm) without sacrificing the high yield of monolayer sheets. The principle of the method is based on the rich intercalation chemistry of graphite oxide (GO).[15,16] Large amounts of GO sediments are formed after a brief oxidation of natural graphite by applying the modified Hummer's method (see Methods). These sediments consist of weakly oxidized graphite which cannot be dispersed well in aqueous solution due to their hydrophobic nature and large size. Our hypothesis is that these large-sized GO aggregates consist of multilayer graphite flakes which are oxidized on the outer layers, while the inner

*Address correspondence to chmlohkp@nus.edu.sg.

Received for review August 28, 2009 and accepted September 23, 2009.

Published online September 29, 2009.
10.1021/nn901111s CCC: $40.75

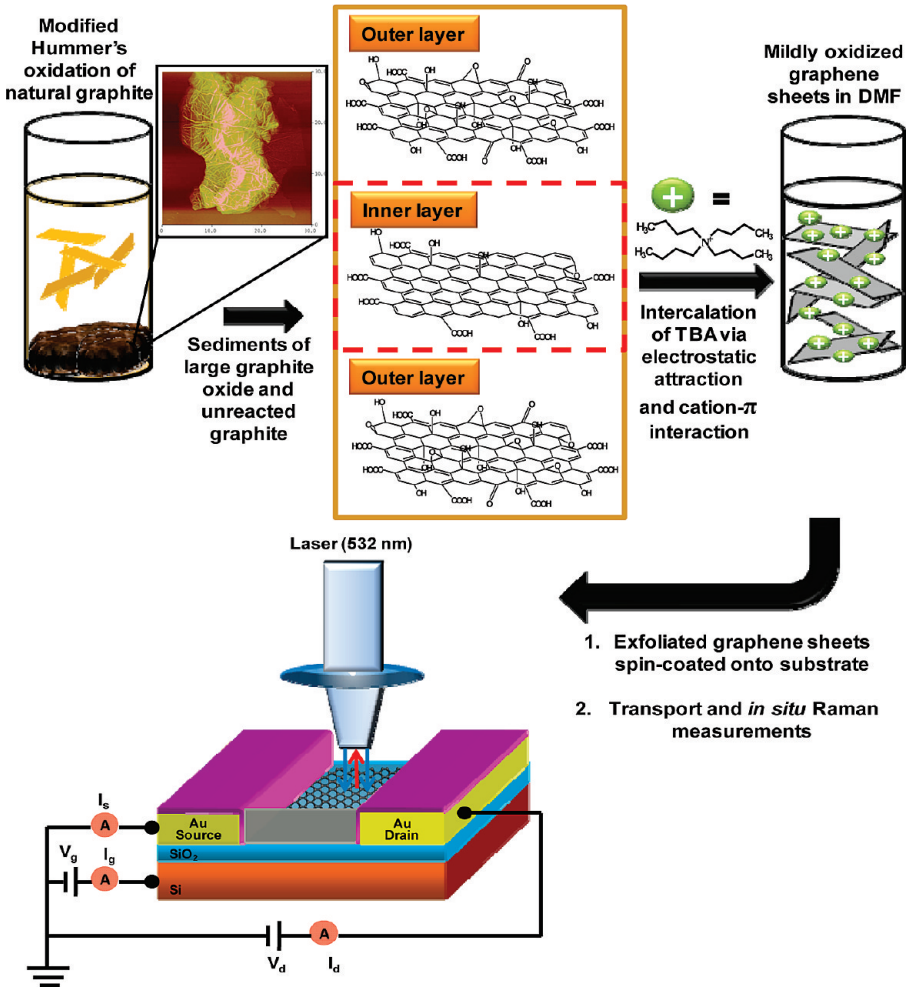

Figure 1. Schematic representation of intercalation of tetrabutylammonium ions in large graphite oxide sediments and unreacted graphite particles to obtain mildly oxidized graphene single sheets in DMF. These exfoliated graphene sheets were deposited onto SiO_2/Si substrate to form thin-film field-effect transistor (FET). Effect of ionic screening and chemical doping effect of NaF and KCl were investigated with electrical transport and *in situ* Raman measurements.

layers consist of pristine or mildly oxidized graphene sheets with oxygen functionalities decorated at the periphery. These aggregated GO sediments were usually discarded by researchers, but here we collected these mildly oxidized GO sediments for further processing with the aim of uncovering the inner pristine or mildly oxidized graphene sheets by performing intercalation−exfoliation chemistry.

RESULTS AND DISCUSSION

Reaction Monitoring of Intercalation−Exfoliation of Graphite Oxide. Figure 1 shows the schematic representation of the intercalation−exfoliation process. The GO sediments collected after centrifugation were intercalated with tetrabutylammonium hydroxide (TBA, 40% in water) under reflux conditions and heated at 80 °C for over 2 days. The quality of exfoliated graphene sheets was determined by UV−vis spectroscopy, X-ray photoelectron spectroscopy (XPS), and electrical conductivity measurements.

The color change of the reaction mixture as the GO sediments were intercalated by TBA over time is shown in Figure 2. Although no chemical reducing agent was used, the intercalation and exfoliation caused the color of the dispersion to change from pale-yellow to dark-brown and, finally, black. The black dispersion is consistent with an overall increase in the UV and visible absorption region, due to the presence of extended π-conjugated structure.[4] The products are hydrophobic but can be dispersed to form a homogeneous suspension in either *N*,*N*-dimethylformamide (DMF) or chloroform after a brief vortex (Figure 2b).[17] The formation of stable dispersion allows the reaction to be monitored by UV−visble absorption spectroscopy. As shown in Figure 2c, the GO sediments displayed an absorption maximum at 231 nm which is due to the $\pi \rightarrow \pi^*$ transition of aromatic C═C bonds and a shoulder at ~290−300 nm which corresponds to the $n \rightarrow \pi^*$ transition of the C═O bond.[18] As the reaction proceeded, the $\pi \rightarrow \pi^*$ (C═C) absorption peak at 231 nm displays a gradual bathochromic shift to 253 nm while the shoulder at ~300 nm for $n \rightarrow \pi^*$ (C═O) absorption peak decreases in intensity. The overall absorption in the whole spectral region increases with reaction time. These changes are comparable to hydrazine reduction of GO, in which a bathochromic shift of 231 nm absorption peak and an increase in background absorbance suggest the restoration of a π-conjugated network within the reduced graphene sheets.[4] We suggest that the increased absorbance is due to the exfoliation of pristine graphene sheets in the interior of the large-sized GO sediments.

The reaction mechanism during the intercalation and exfoliation was further investigated by X-ray photoelectron spectroscopy (XPS). As shown in Figure 2d, the percentage of C−C bonds increases from 55% after 1 h to 81% after 2 days. The increase in the C−C component and corresponding decrease in C−O (epoxide, ether, and hydroxyl groups) and C═O (carbonyl and carboxyl) components with reaction time indicate the generation of large domains of π-conjugated structures. By comparing the relative peak heights of the C−O *versus* C−C peak, we conclude that these TBA-

intercalated graphene sheets have a smaller percentages of nonstoichiometric (10% oxidized C) oxidized G compared to GO obtained by the modified Hummer's method.[19]

The chemical exfoliation of the large GO sediments is inherently selective. The outer layers of highly oxidized graphene sheets with a larger proportion of oxygen functionalities will be exfoliated first due to greater interlayer distance and weaker van der Waals interactions, which afford greater ease of TBA insertion.[15,16] This is followed by exfoliation of the less oxidized inner sheets in which the oxygen functionalities are situated mainly at the graphene edge planes. Due to different solubilities, the highly oxidized graphene sheets (yellow-brown in color) could be separated from the less oxidized graphene sheets by centrifugation (1500 rpm for 30 min) (see Methods). Subsequent purification resulted in a homogeneous black dispersion of mildly oxidized graphene sheets (Figure 2b).

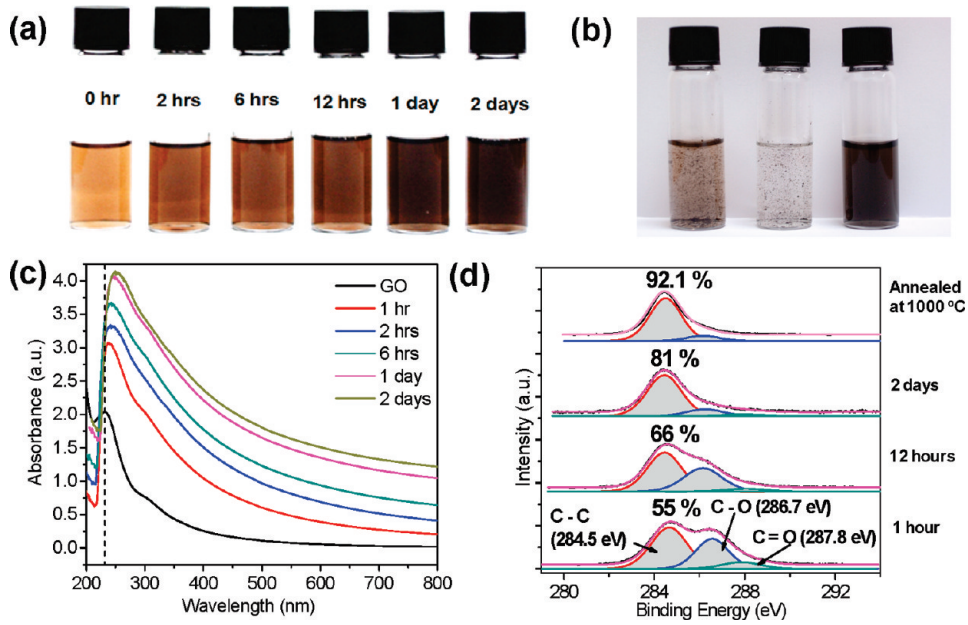

Figure 2. Reaction monitoring of TBA intercalation in large graphite oxide particles. (a) Color change of reaction mixture in DMF monitored over 2 days. Suspension was centrifuged at 10 000 rpm for 10 min to remove unreacted particles. (b) Precipitation of relatively hydrophobic mildly oxidized graphene sheets in deionized water after reaction for 1 day (left) and 2 days (center) and redispersion in DMF (right). (c) UV−vis absorption spectra of GO dispersions as reaction proceeded for over 2 days. (d) C 1s XPS spectra of GO dispersion with reaction time show gradual increase in the C−C bonding component from 50 to 80%.

After spin-coating on substrate, a good monolayer yield of ~90% can be obtained from our graphene dispersions with a mean sheet area of 330 ± 10 μm^2, as can be seen in the optical micrograph and atomic force microscope topography study in Figure 3. The average topographical height obtained using AFM was ~0.93 nm, which is comparable to the reported height of graphene sheets possessing residual oxygen functionalities (Figure 3b−d).[3,4,6] A good indicator of the presence and effective restoration of π-conjugated domains on graphene sheet is electrical conductivity. Unlike the GO prepared by Hummer's method, which is electrically insulating, the graphene sheets produced directly by this intercalation−exfoliation method exhibit appreciable conductivity. Single-sheet graphene FET devices fabricated using these graphene sheets displayed an average sheet conductivity of 2 ± 1 S/m prior to thermal reduction. These mildly oxidized graphene sheets were

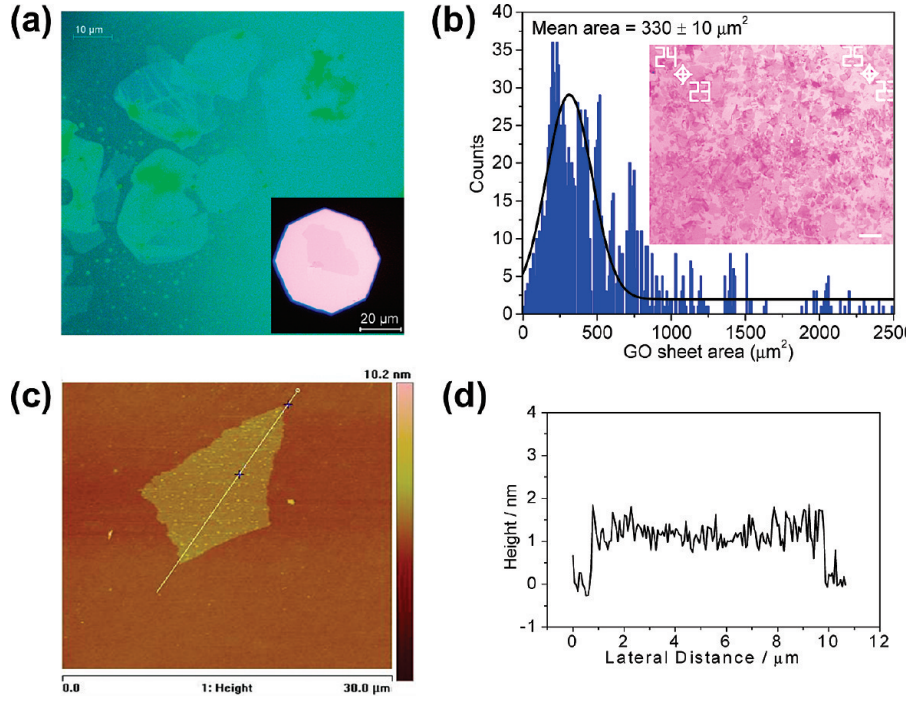

Figure 3. Optical micrograph and tapping mode AFM characterization of exfoliated mildly oxidized graphene sheet. (a) Optical image of large-sized mildly oxidized graphene sheets. (b) Size distribution of single-layer graphene sheets (total counts = 1435) with mean sheet area of 330 ± 10 μm^2. Inset shows a good spread of monolayer graphene sheets with some overlapping regions; scale bar is 50 μm. The total number of sheets counted was ~1600, of which 1435 sheets were single-layer. (c) Tapping mode AFM image of a single sheet of mildly oxidized graphene sheet. (d) Topographical height for mildly oxidized graphene sheet is ~0.93 nm, which is larger than reduced graphene sheet due to the presence of protruding oxygen functionalities.

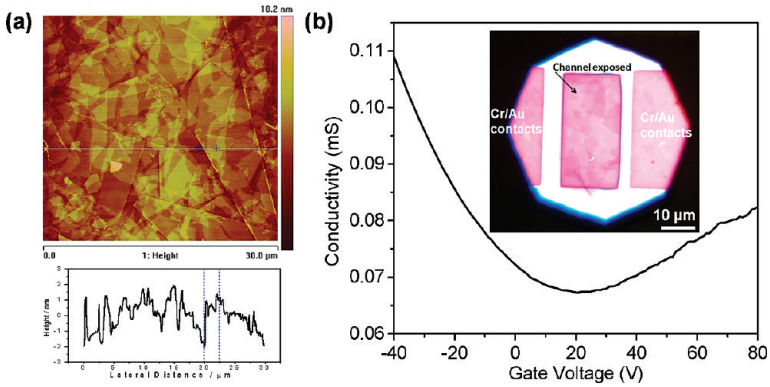

Figure 4. Characterization of graphene film thickness and morphology. (a) Tapping mode AFM characterization of graphene film with film thickness ~ 3 nm prior to annealing. (b) $\sigma - V_g$ characteristics of thin graphene film (approximately 1−4 layers) with sheet conductivity of 15 000 S/m and hole and electron mobility of 59 and 17 $cm^2/(V \cdot s)$, respectively. Inset shows two-point probe configuration of thin-film graphene-based field-effect transistor (FET) with PMMA insulation of contacts and active channel area exposed by electron beam lithography. Channel length and width is 29.3 and 37.8 μm, respectively.

thermally reduced by annealing at 1000 °C to restore its π-conjugated structure. After reduction, a high C−C percentage of 92% is achieved as judged from the C 1s peak profile in XPS (Figure 2d).[3] Furthermore, the disappearance of the N 1s peak, which is indicative of the presence of organic ammonium groups in TBA cations, suggests the effective removal of TBA cations by thermal annealing (see Supporting Information, S2). Upon thermal annealing at 1000 °C, sheet conductivity increases to ~3210 S/m (see Supporting Information, S3).

Characterization of Thin Graphene Film Field-Effect Transistor. The ability to form uniform large-area conductive graphene film exhibiting high field-effect transistor mobility is needed for application in electronics. The mildly oxidized graphene sheets are poorly dispersed in deionized water. Dispersion of these graphene sheets in DMF gives the most stable colloidal suspension. The high boiling point of DMF (153 °C) necessitates a preheating of the SiO_2/Si substrate to 350 °C before spin-coating.[20] By using an optimal concentration of 0.5 mg/mL and spin-coating speed of 3000 rpm, a reasonably uniform graphene film could be formed on the SiO_2/Si substrate. The number of graphene layers was accurately determined using tapping mode AFM, Raman and optical contrast spectroscopy to eliminate any instrument offset problem. Figure 4a shows that the spin-coated graphene film consisted of a majority 2 to 3 layers of graphene sheets with thickness of ~3 nm (individual sheet height is ~0.93 nm) prior to heating. After thermal annealing, graphene film thickness was reduced to ~1.5 nm, verified using Raman and optical contrast spectroscopy (see Supporting Information, S4).[21]

The electronic properties of the graphene films were measured using a two-probe configuration. The areas surrounding the graphene active channel were etched by oxygen plasma to reduce gate leakage current. The gate leakage current for all of our devices is limited to 300 pA. The graphene films produced here show a conductivity of ~15 000 S/m and hole and electron mobilities of 59 and 17 $cm^2/(V \cdot s)$, respectively (Figure 4b). When the channel length is increased to 100 μm, carrier mobilities are reduced by ~4−5 times, thus suggesting that sheet-to-sheet junction is one of the limiting factors for carrier mobilities (see Supporting Information, S5).

Ionic Screening Effect on Graphene Transistor Performance. Charge carrier mobility is one of the most important issues in transistor performance. Therefore, the factors which limit the FET carrier mobility in our intercalation−exfoliation graphene sheets, other than sheet-to-sheet junction, are investigated here. The asymmetric "V" shape of the drain−source current (or conductivity) *versus* gate voltage plot, which characterizes such samples, reflects the presence of charged impurities which impart p-type electrical characteristics to these films. These charged impurities originate from trapped charges in the oxide layer or at the graphene−oxide interface.[22] Negatively charged impurities and $Si-O^-$ groups have been found to dope single-layer graphene[23] and organic thin-film transistors.[24] This effect is especially deleterious at the Dirac point (which defines the threshold voltage) since the screening is weak due to lower carrier concentration. Chen *et al.* demonstrated that long-range scattering due to charged impurities could be reduced by dielectric screening *via* ionic solutions[25,26] or high dielectric constant liquids on mechanically cleaved graphene.[27] Mobility enhancement of over 1 order of magnitude was observed for all of their devices as the concentration of ionic solution or dielectric constant of liquids increased. Du *et al.* showed that suspended graphene could reach a high mobility of 200 000 $cm^2/(V \cdot s)$ at low temperature when carrier density was reduced to ~10^9 cm^{-2}.[28] It is not known what are the main factors restricting the carrier mobility in chemically processed graphene below the 1000 $cm^2/(V \cdot s)$ range. A multitude of factors such as impurity doping, presence of structural defects and scattering centers, and sheet-to-sheet junctions may be limiting. To investigate if ionic screening could improve the carrier mobility, we performed back-gating *via* SiO_2 in the presence of NaF or KCl electrolyte on top of the channel. It is anticipated that anions such as F^- and Cl^- will show different adsorption behavior on the graphene surface.[29] The driving force for ion adsorption on a hydrophobic surface such as graphene arises from favorable interactions between the charge density oscillations of structured water at the interface and the permanent and induced dipoles of the molecular ions. Polarizable ions such as Cl^- are well-known to exhibit specific adsorption on a wide range of surfaces and can approach the graphene sur-

face closely by interacting with the structured water layers. This short-range specific interaction can be strong enough to withstand opposing Coulombic field induced by negatively charged impurities on SiO_2. On the other hand, nonpolarizable ions such as F^- do not approach the surface as closely and may be repelled by negatively charged impurities, although they can contribute to the overall dielectric strength of the solution.

Figure 5a shows the $\sigma - V_g$ characteristic of graphene film operated with a back gate configuration with the channel exposed to NaF electrolyte. When the NaF concentration is increased from 10 mM to 1 M, there is a sharp increase in the slope of the $\sigma - V_g$ plot, which suggests either a doping effect which increases carrier concentration or an ionic screening effect which improves the carrier mobility. A parallel study with *in situ* Raman spectroscopy (discussed later) indicates that the carrier concentration in the graphene film has, in fact, decreased with increasing ionic strength of the solution. This suggests that the sharp increase in conductivity arises mainly from the effects of dielectric screening of impurity doping. Another evidence, which echoes this trend, is the progressive shift of the gate voltage at the minimum conductivity ($V_{g,min}$) (also known as threshold voltage) toward zero gate voltage as the concentration of NaF increases, and this is accompanied by a sharpening of the $\sigma - V_g$ slope. This shift in $V_{g,min}$ can be used to calculate the change in doping concentration. The application of gate voltage (V_g) across 285 nm of SiO_2 creates an electrostatic potential difference (φ) between graphene and SiO_2 back gate. For back gate, $V_g \approx \varphi = ne/C_g$, where n is the carrier concentration in units of cm^{-2}, e is elementary charge, and C_g is the geometrical capacitance.[30] Therefore, we can estimate the excess or depletion of hole (electron) concentration by $V_g - V_{g,min} = ne/C_g$, in which a negative (positive) $V_g - V_{g,min}$ induces holes (electrons). Taking $V_g = 0$ V to be the reference point for undoped graphene, a negative shift of $V_{g,min}$ from positive voltage toward zero voltage indicates a decreasing hole concentration (smaller $|V_g - V_{g,min}|$ value). Therefore, on the basis of the transport measurements taken at $V_g = 0$ V, the hole carrier density in graphene decreased from 1.5×10^{12} cm^{-2} in dry conditions to 2.8×10^{11} cm^{-2} in 1 M NaF, which is comparable to the estimated sheet carrier density in suspended graphene.[31] In addition, on the basis of the change in the slope of the $\sigma - V_g$ plot, an increase in hole mobility from 59 to 460 $cm^2/(V \cdot s)$ and increase in electron mobility from 17 to 310 $cm^2/(V \cdot s)$ can be estimated. There is also an apparent reduction in the asymmetry of the $I - V$ curve for holes *versus* electrons and an increase in the I_{on}/I_{off} ratio from 1.5 to 10.

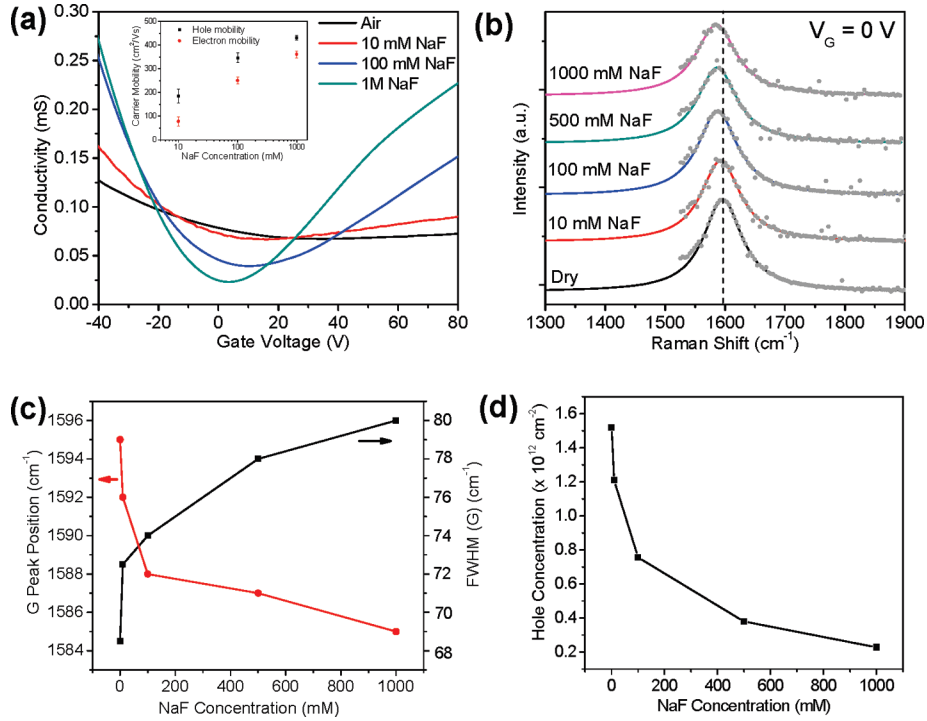

Figure 5. Ionic screening effect of NaF ionic solution. (a) Transfer characteristics of a thin-film graphene-based device in different NaF concentration. V_{ds} is kept constant at 10 mV. Inset shows mobility (indicated by the slope of $\sigma - V_g$ curve) increases with NaF concentration, which is indicative of effective ionic screening of charged impurities on SiO_2 substrate. (b) Raman spectra show G-mode response fitted with Lorentzian component of the Voigt profile in different NaF concentrations. (c) G peak down-shifted by ~8 cm^{-1}, and line width increased by ~12 cm^{-1}. (d) Hole carrier concentration decreases from 1.5×10^{12} cm^{-2} in dry conditions to 2.8×10^{11} cm^{-2} in 1 M NaF.

The decrease in the concentration of impurity dopants in the graphene when the ionic strength of the NaF gating electrolyte was varied systematically was verified using *in situ* Raman spectroscopy. The position of the G peak and its line width (full width at half-maximum) are highly sensitive to changes in carrier concentration; the G peak up-shifts, and its line width decreases for both holes and electron doping. The line width of the G peak is proportional to the statistical availability for electron−hole pair generation at the G peak energy. This can be expressed in this equation:[32]

$$\Gamma_G = \Gamma_0 + \Delta\Gamma f_T\left[\frac{\left(\frac{-\hbar\omega_G}{2 - E_F}\right)}{\left(\frac{\hbar\omega_G}{2 - E_F}\right)}\right]$$

where $\Delta\Gamma$ corresponds to the maximum phonon broadening from electron−hole pair generation, f_T is the Fermi−Dirac distribution at temperature T, E_F is the Fermi energy with respect to the Dirac point in graphene, Γ_0 is the line width contribution from

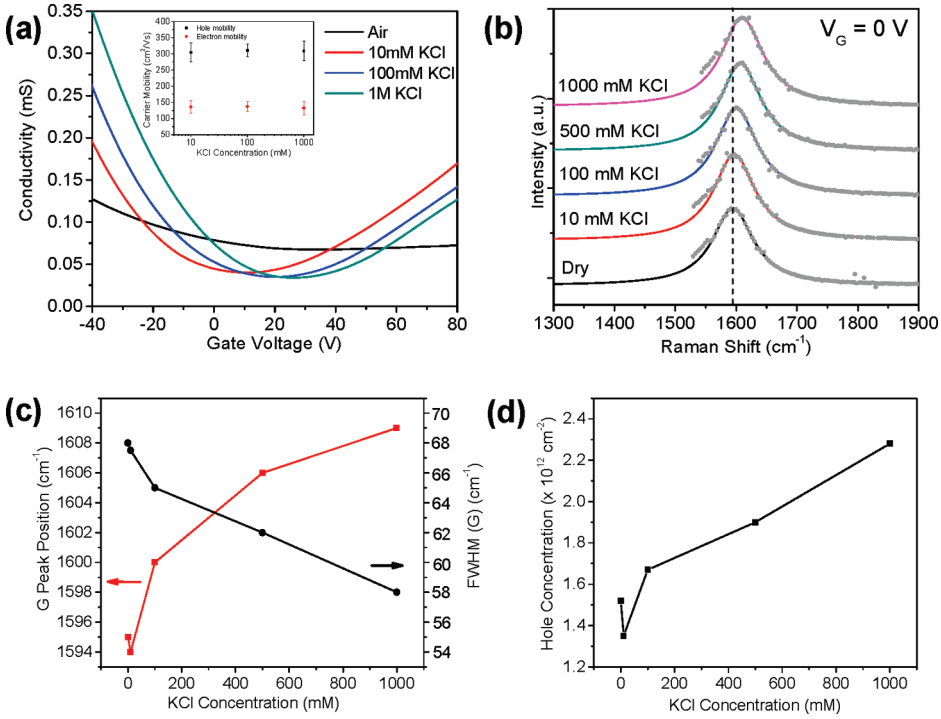

Figure 6. Ionic screening effect of KCl ionic solution. (a) Transfer characteristics of graphene film in different KCl concentrations. V_{ds} is kept constant at 10 mV. Threshold voltage shifts toward positive gate voltages. Inset shows that carrier mobilities increase initially and remain constant as KCl concentration increases beyond 10 mM. (b) Raman spectra show G-mode response fitted with Lorentzian component of the Voigt profile in different KCl concentrations. (c) G peak up-shifts by ~12 cm^{-1}, and line width decreases by ~10 cm^{-1}. (d) Initial slight decrease in hole carrier when the graphene FET is exposed to 10 mM KCl, but it gradually increases to 2.3 × 10^{12} cm^{-2} in 1 M KCl.

phonon−phonon coupling and other factors independent of electronic interactions. Therefore, a narrowing of the line width of the G-mode reflects an increasing number of electron−hole pairs.

In addition, the ratio of the intensities of the G and 2D peaks (I_{2D}/I_G) also shows a strong dependence on doping, thus affording sensitive monitoring of changes in dopant concentration.[30,31] A recent in-depth theoretical study suggests that, while the G peak intensity does not depend on doping, the 2D peak intensity is sensitive to carrier concentration and decreases with increasing carrier concentration due to scattering effect on carrier mobilities.[33] The initial G peak position of our graphene sample is situated at 1595 cm^{-1} before exposure to the ionic solution; this is up-shifted by ~10 cm^{-1} from undoped graphene[31] and reflects p-doping by the substrate. This p-doping agrees with the $\sigma-V_g$ characteristics where the threshold voltage of the graphene sample is at ~20 V before ionic screening. As shown in Figure 5c, the down-shifting of the G peak by ~8 cm^{-1} and increase in line width of the G peak by ~12 cm^{-1} with increasing ionic strength of the NaF gating electrolyte suggest a reduction in carrier concentration. The increase in the ratio of the integrated intensity of 2D to G modes (I_{2D}/I_G) by ~8 times with an increase in NaF concentration is also reflective of a decrease in carrier concentration in the graphene (see Supporting Information, S7). Therefore, the changes in the G- and 2D-mode responses indicate a gradual decrease in substrate-induced holes in graphene with increasing NaF concentration, as shown in the plot in Figure 5d. This is clearly evident of the ionic screening mechanism which counteracts the p-type impurity doping by the SiO_2 substrate.

The use of KCl as the gating electrolyte reveals a different response from NaF in several aspects. Figure 6a shows the $\sigma-V_g$ characteristic of graphene film in different KCl concentrations. As the concentration of KCl increases, the slope of the $\sigma-V_g$ increases sharply in the beginning similar to the NaF case. The hole and electron mobilities increase initially from 59 to 300 $cm^2/(V\cdot s)$ and from 17 to 130 $cm^2/(V\cdot s)$, respectively. However, one interesting difference is that, above 10 mM concentration, the slope of the $\sigma-V_g$ plot does not change, but $V_{g,min}$ now shifts toward positive gate voltages. In view of the fact that Cl^- ions can show specific adsorption on hydrophobic surfaces, we propose there is interplay between screening and doping effect of KCl, which is concentration-dependent. The screening effect is clearly evident from the slight negative shift of $V_{g,min}$ from 20 to 17 V and slight down-shift of the G peak by ~1 cm^{-1}, as monitored by Raman spectroscopy when graphene is exposed to 10 mM KCl (Figure 6b,c). At higher KCl concentration, the chemical doping effect of Cl^- ions outweighed that of ionic screening, and this is evidenced by the shift of $V_{g,min}$ toward positive gate voltages. This is manifested by the gradual up-shifting of the G peak toward higher frequency (~12 cm^{-1}) and the decrease in line width of the G peak by ~10 cm^{-1} (Figure 6b). From Raman and transport measurements taken at V_g = 0 V, we obtained an estimated increase in hole carrier density from 1.5 × 10^{12} cm^{-2} in dry conditions to 2.3 × 10^{12} cm^{-2} in 1 M KCl (Figure 6d).

CONCLUSIONS

We have demonstrated an approach to obtain conducting graphene sheets based on the intercalation and exfoliation of GO sediments with tetrabutylammonium ions. A homogeneous colloidal suspension of mildly oxidized graphene sheets, coupled with a high monolayer yield (~ 90%), allows it to be used for device fabrication.

We demonstrated that impurity doping by the substrate reduces the intrinsic field-effect transistor carrier mobility of such chemically processed graphene film by at least an order. Using NaF for ionic screening, the mobility of the graphene can be improved by one order from the unscreened situation in dry air. From electrical transport measurement and *in situ* Raman spectroscopy, we found that the dopant concentration is reduced from 1.5×10^{12} to 2.8×10^{11} cm^{-2}, and as a consequence, the hole mobility is increased from 59 to 460 $cm^2/(V \cdot s)$ and electron mobility is increased from 17 to 310 $cm^2/(V \cdot s)$. We also show that the effect of the ionic electrolyte depends on the specific property of the ions. In the case of KCl, there is a concentration-dependent interplay of ionic screening and chemical doping, which may arise from specific adsorption of the Cl^- at the graphene−water interface.

METHODS

Oxidation of Natural Graphite and Intercalation by Tetrabutylammonium Ions. Graphite (1.5 g), $NaNO_3$ (1.5 g), and H_2SO_4 (69 mL) were mixed and stirred in an ice bath. Next, 9 g of $KMnO_4$ was slowly added. The reaction mixture was then stirred in room temperature for 1 h. After which, 100 mL of water was added and the temperature was increased to 90 °C for 30 min. Finally, 300 mL of water was slowly added, followed by another slow addition of 10 mL of 30% H_2O_2. The reaction mixture was filtered and washed with water until the pH was about 6. The graphite oxide precipitate was dispersed in water/methanol (1:5) mixture and purified with three repeated centrifugation steps at 12 000 rpm for 30 min. The purified sample was then dispersed in deionized water and centrifuged at 2500 rpm to separate single-sheet highly oxidized graphene sheets in the supernatant from mildly oxidized graphite oxide and some unreacted graphite sediments found at the bottom. These sediments (roughly 0.5 g) were recovered, dried, and dispersed in 20 mL of *N*,*N*-dimethylformamide (DMF) and 2 mL of tetrabutylammonium hydroxide solution (40% water). The mixture was then heated under reflux at 80 °C for over 2 days. A black suspension resulted, which remained stable for 6 months without precipitation. To recover single sheets of mildly oxidized graphene sheets, the reaction mixture was purified with repeated centrifugation in water/methanol (1:5) mixture as above, followed by a fresh addition of DMF for the last purification step. The final purified sample was dispersed in DMF. Centrifugations at 1500 rpm for 30 min were used to isolate highly oxidized outer layers of GO (supernatant) from mildly oxidized ones (bottom). A good monolayer yield of ~90% was obtained, confirmed by tapping mode atomic force microscopy.

Fabrication and Electrical Measurements of Graphene FET. Single-layer GO sheets were spin-coated on oxidized silicon substrates (285 nm SiO_2 with prefabricated marker) and annealed at 1000 °C. The samples were identified and located by optical microscopy. One hundred microliters of 3% poly(methyl methacrylate) (PMMA) (molecular mass, 950 K) chlorobenzene solution was spin-coated on substrates at 6000 rpm using Spincoater Model P6700 Series (Specialty Coating Systems, Inc.) and baked at 120 °C for 15 min. The thickness of PMMA is about 200 nm. Electron-beam lithography was done using a Philips XL30 FEGSEM at 30 kV with a Raith Elphy Plus controller, with an exposure dosage of 280 $\mu A/cm^2$. The PMMA was then developed with a methyl isobutyl keton (MIBK) and isopropyl alcohol (1:3) solution. Ten nanometer chromium and 100 nm gold were deposited in the substrate through thermal evaporation. The films were then lifted off in acetone at room temperature and rinsed with isopropyl alcohol. The Cr/Au contacts were annealed at 350 °C in a vacuum furnace for 40 min to improve the contacts between metal and graphene. The transport measurements for devices were obtained with a B1500A Semiconductor Device Analyzer (Agilent Technologies) using the in-built R-I Kelvin measurement software. Electron and hole mobility can be extracted from the linear regime of the transfer characteristics using $\mu = [(\Delta I_{ds}/V_{ds}) \times (L/W)]/C_{ox}\Delta V_g$, where L and W are channel length and width, respectively, C_{ox} is silicon oxide gate capacitance (which is 1.21×10^{-8} F/cm^2 for a gate oxide thickness of 285 nm), and I_{ds}, V_{ds}, and V_g are drain−source current, drain−source voltage, and gate voltage, respectively. To allow for electrolyte gating of the channel, the contacts were insulated by spin-coating the device with a layer of PMMA photoresist baked at 150 °C and selectively exposing the channel area by electron-beam lithography. The graphene channel was exposed by developing with a MIBK and isopropyl alcohol (1:3) solution (see Figure 4b).

Raman Spectroscopy. The Raman spectra were obtained with a WITEC CRM200 Raman system. The excitation source is 532 nm laser (2.33 eV) with a laser power below 0.1 mW to avoid laser-induced heating. The laser spot size at focus was around 500 nm in diameter with a 100× objective lens (NA = 0.95). Spectral resolution is 4 cm^{-1}. All G- and D-mode features were adequately fitted with a Lorentzian component of the Voigt profiles. All Raman spectra in Figure 5 and 6 exhibited a prominent G peak which relates to the E_{2g} vibrational mode between sp^2 carbon. D-mode, which relates to an out-of-plane vibrational mode, indicative of sp^3 carbons in the surroundings, is left out for clearer representation of G-mode response in NaF and KCl concentrations. The ratio of integrated intensity of D- and G-mode (I_D/I_G) for thermally annealed graphene sheets ranges from 0.81 to 1.1, thus indicating homogeneity and good restoration of π-conjugated structure.[3]

Acknowledgment. The authors thank the support of NRF-CRP grant "Graphene Related Materials and Devices" R-143-000-360-281.

Supporting Information Available: XPS spectra of annealed graphene sheets, electrical characterization of single graphene flake, Raman, optical contrast spectroscopy, and transport measurement of graphene film, *etc.* This material is available free of charge *via* the Internet at http://pubs.acs.org.

REFERENCES AND NOTES

1. Novoselov, K. S.; Geim, A. K.; Morozov, S. V.; Jiang, D.; Zhang, Y.; Dubonos, S. V.; Grigorieva, I. V.; Firsov, A. A. Electric Field Effect in Atomically Thin Carbon Films. *Science* **2004**, *306*, 666–669.
2. Geim, A. K.; Novoselov, K. S. The Rise of Graphene. *Nat. Mater.* **2007**, *6*, 183–191.
3. Gao, W.; Alemany, L. B.; Ci, L.; Ajayan, P. M. New Insights into the Structure and Reduction of Graphite Oxide. *Nat. Chem.* **2009**, *1*, 403–408.
4. Li, D.; Müller, M. B.; Gilje, S.; Kaner, R. B.; Wallace, G. G. Processable Aqueous Dispersions of Graphene Nanosheets. *Nat. Nanotechnol.* **2007**, *3*, 101–105.
5. Tung, V. C.; Allen, M. J.; Yang, Y.; Kaner, R. B. High-Throughput Solution Processing of Large-Scale Graphene. *Nat. Nanotechnol.* **2008**, *4*, 25–29.
6. Li, X.; Zhang, G.; Bai, X.; Sun, X.; Wang, X.; Wang, E.; Dai, H. Highly Conducting Graphene Sheets and Langmuir−Blodgett Films. *Nat. Nanotechnol.* **2008**, *3*, 538–542.
7. Gu, W.; Zhang, W.; Li, X.; Zhu, H.; Wei, J.; Li, Z.; Shu, Q.; Wang, C.; Wang, K.; Shen, W.; Kang, F.; Wu, D. Graphene Sheets from Worm-like Exfoliated Graphene. *J. Mater. Chem.* **2009**, *19*, 3367–3369.
8. Lotya, M.; Hernandez, Y.; King, P. J.; Smith, R. J.; Nicolosi, V.; Karlsson, L. S.; Blighe, F. M.; De, S.; Wang, Z.; McGovern, I. T.; Duesberg, G. S.; Coleman, J. N. Liquid Phase Production of Graphene by Exfoliation of Graphite in Surfactant/Water Solutions. *J. Am. Chem. Soc.* **2009**, *131*, 3611–3620.

9. Hernandez, Y.; Nicolosi, V.; Lotya, M.; Blighe, F. M.; Sun, Z.; De, S.; McGovern, I. T.; Holland, B.; Byrne, M.; Gun'ko, Y. K.; Boland, J. J.; Niraj, P.; *et al.* High-Yield Production of Graphene by Liquid-Phase Exfoliation of Graphite. *Nat. Nanotechnol.* **2008**, *3*, 563–568.
10. Biswas, S.; Drzal, L. T. A Novel Approach to Create a Highly Ordered Monolayer Film of Graphene Nanosheets at the Liquid-Liquid Interface. *Nano Lett.* **2009**, *9*, 167–172.
11. Ang, P. K.; Chen, W.; Wee, A. T. S.; Loh, K. P. Solution-Gate Epitaxial Graphen as pH Sensor. *J. Am. Chem. Soc.* **2008**, *130*, 14392–14393.
12. Emtsev, K. V.; Bostwick, A.; Horn, K.; Jobst, J.; Kellogg, G. L.; Ley, L.; McChesney, J. L.; Ohta, T.; Reshanov, S. A.; Röhrl, J.; *et al.* Towards Wafer-Size Graphene Layers by Atmospheric Pressure Graphitization of Silicon Carbide. *Nat. Mater.* **2009**, *8*, 203–207.
13. Obraztsov, A. N. Chemical Vapour Deposition: Making Graphene on a Large Scale. *Nat. Nanotechnol.* **2009**, *4*, 212–213.
14. Luo, Z. T.; Lu, Y.; Somers, L. A.; Johnson, A. T. C. High Yield Preparation of Macroscopic Graphene Oxide Membranes. *J. Am. Chem. Soc.* **2009**, *131*, 898–899.
15. Liu, Z.-H.; Wang, Z.-M.; Y, X.; Ooi, K. Intercalation of Organic Ammonium Ions into Layered Graphite Oxide. *Langmuir* **2002**, *18*, 4926–4932.
16. Simonet, J.; Lund, H. Electrochemical Behaviour of Graphite Cathodes in the Presence of Tetraalkylammonium Cations. *J. Electroanal. Chem.* **1977**, *75*, 719–730.
17. Park, S.; An, J.; Jung, I.; Piner, R. D.; An, S. J.; Li, X.; Velamakanni, A.; Ruoff, R. S. Colloidal Suspensions of Highly Reduced Graphene Oxide in a Wide Variety of Organic Solvents. *Nano Lett.* **2009**, *9*, 1593–1597.
18. Clark, B. J.; Frost, T.; Russell, M. A. *UV Spectroscopy: Techniques, Instrumentation, Data Handling/UV Spectrometry Group*; Chapman & Hall: London, NY, 1993; Vol. 4.
19. Stankovich, S.; Dikin, D. A.; Piner, R. D.; Kohlhaas, K. A.; Kleinhammes, A.; Jia, Y. Y.; Wu, Y.; Nguyen, S. T.; Ruoff, R. S. Synthesis of Graphene-Based Nanosheets *via* Chemical Reduction of Exfoliated Graphite Oxide. *Carbon* **2007**, *45*, 1558–1565.
20. Blake, P.; Brimicombe, P. D.; Nair, R. R.; Booth, T. J.; Jiang, D.; Schedin, F.; Ponomarenko, L. A.; Morozov, S. V.; Gleeson, H. F.; Hill, E. W.; Geim, A. K.; Novoselov, K. S. Graphene-Based Liquid Crystal Device. *Nano Lett.* **2008**, *8*, 1704–1708.
21. Ni, Z. H.; Wang, H. M.; Kasim, J.; Fan, H. M.; Wu, Y. H.; Feng, Y. P.; Shen, Z. X. Graphene Thickness Determination Using Reflection and Contrast Spectroscopy. *Nano Lett.* **2007**, *7*, 2758–2763.
22. Fowkes, F. M.; Burgess, T. E. Electric Fields at the Surface and Interface of SiO_2 Films on Silicon. *Surf. Sci.* **1969**, *13*, 184–195.
23. Casiraghi, C.; Pisana, S.; Novoselov, K. S.; Geim, A. K.; Ferrari, A. C. Raman Fingerprint of Charged Impurities in Graphene. *Appl. Phys. Lett.* **2007**, *91*, 233108.
24. Chua, L.-L.; Zaumseil, J.; Chang, J.-F.; Ou, E. C.-W.; Ho, P. K.-H.; Sirringhaus, H.; Friend, R. H. General Observation of n-Type Field-Effect Behaviour in Organic Semiconductors. *Nature* **2005**, *434*, 194–199.
25. Chen, F.; Xia, J.; Tao, N. Ionic Screening of Charged-Impurity Scattering in Graphene. *Nano Lett.* **2009**, *9*, 1621–1625.
26. Chen, F.; Qing, Q.; Xia, J.; Li, J.; Tao, N. Electrochemical Gate-Controlled Charge Transport in Graphene in Ionic Liquid and Aqueous Solution. *J. Am. Chem. Soc.* **2009**, *131*, 9908–9909.
27. Chen, F.; Xia, J.; Shishir, R.; Ferry, D. K.; Tao, N. Dielectric Screening Enhanced Performance in Graphene FET. *Nano Lett.* **2009**, *9*, 2571–2574.
28. Du, X.; Skachko, I.; Barker, A.; Andrei, E. Y. Approaching Ballistic Transport in Suspended Graphene. *Nat. Nanotechnol.* **2008**, *3*, 491–495.
29. Bard, A. J.; Faulkner, L. R. *Electrochemical Methods: Fundamentals and Applications*, 2nd ed.; John Wiley & Sons: New York, 2001; pp 554−557.
30. Das, A.; Pisana, S.; Chakraborthy, B.; Piscanec, S.; Saha, S. K.; Waghmare, U. V.; Novoselov, K. S.; Krishnamurthy, H. R.; Geim, A. K.; Ferrari, A. C.; Sood, A. K. Monitoring Dopants by Raman Scattering in an Electrochemically Top-Gated Graphene Transistor. *Nat. Nanotechnol.* **2008**, *3*, 210–215.
31. Berciaud, S.; Ryu, S.; Brus, L. E.; Heinz, T. F. Probing the Intrinsic Properties of Exfoliated Graphene: Raman Spectroscopy of Free-Standing Monolayers. *Nano Lett.* **2009**, *9*, 346–352.
32. Lazzeri, M.; Mauri, F. Nonadiabatic Kohn Anomaly in a Doped Graphene Monolayer. *Phys. Rev. Lett.* **2006**, *97*, 266407.
33. Basko, D. M. Theory of Resonant Multiphonon Raman Scattering in Graphene. *Phys. Rev. B* **2008**, *78*, 125418.